Assessment of fluctuation-induced and wall-induced anomalous electron transport in HET

IEPC-2015-418／ISTS-2015-b-418

Presented at Joint Conference of 30th International Symposium on Space Technology and Science
34th International Electric Propulsion Conference and 6th Nano-satellite Symposium,
Hyogo-Kobe, Japan
July 4 – 10, 2015

Francesco Taccogna[1] and Pierpaolo. Minelli[2]
P.Las.M.I. Lab@CNR-NanoTec, Bari, 70126, Italy

In this work, an assessment of the different contributions to the anomalous electron transport in a Hall-effect thruster (HET) channel discharge was carried out through a fully kinetic 3D PIC-MCC model. The fluctuation-induced and near-wall-induced contributions have been separately estimated turning off the secondary electron emission and the azimuthal direction, respectively, and comparing these two cases with the full (including all the mechanisms) case. Results show that the near-wall-conductivity contributes to 60% of the total axial electron current detected at the anode while the azimuthal fluctuation account for only 20%.

Nomenclature

B	=	magnetic field
f	=	geometrical scaling factor
E	=	energy
I	=	current
I_D	=	discharge current
j	=	current density
k	=	wave number
n	=	density
r	=	radial direction
r_{in}	=	inner radius of the channel
z	=	axial direction
γ	=	total secondary electron emission coefficient
Δt	=	time step
θ	=	azimuthal direction
π	=	pi-greek
ρ	=	charge density
σ	=	surface charge density
ϕ	=	electric potential
ω_p	=	electron plasma frequency

I. Introduction

The entire functioning principle of Hall-effect thruster (HET) is based on the electron transport in ***E***x***B*** field[1]. It is well recognized that this discharge configuration creates high anisotropy and azimuthal fluctuations. In addition,

[1] Permanent Researcher, Consiglio Nazionale delle Ricerche, francesco.taccogna@cnr.it.
[2] Permanent Researcher, Consiglio Nazionale delle Ricerche, pierpaolo.minelli@cnr.it.

the lateral surfaces play an active role due to the strong secondary electron emission in the acceleration region of the channel inducing space-charged saturated or even inverted sheaths. Both mechanisms, azimuthal fluctuations and electron-wall interaction, are responsible of the anomalous electron cross-field transport consisting in an axial electron current 10 times larger than the collision-induced current.

Due to the low collisionality, both mechanisms have a strong kinetic character and any fluid treatment with an *ad hoc* fitting electron mobility is not helpful for understanding the real nature of electron transport and consequently for optimizing the HET current efficiency.

For this reason, in the last decade, thanks to new computer technologies and high performance programming (CUDA NVIDIA, Intel Xeon Phi coprocessor, etc.), 2D and 3D Particle-in-Cell (PIC) models of HET have begun to appear on the international scene[2-5]. The realistic and complex nature of these *ab initio* models has meant that they were called numerical experiments, but as such, they does not allow to investigate in detail the physics of HET. For this reason, in the present work, the fully kinetic three-dimensional PIC model have been developed allowing to isolate one aspect at a time before to combine them all together. In particular, three different cases have been invetigated and compared:

- case A: 3D(r,θ,z) representation of the HET discharge
- case B: 2D(r,z) axisymmetric representation
- case C: 3D(r,θ,z) representation without SEE (completely absorbing lateral walls).

Comparison between cases A and B will show the contribution of the azimuthal fluctuation on the electron transport, while comparison between cases A and C will point out the effects of electron-surface interaction on the electron current.

The paper is organized as follows: in the next section, the model is outlined, while in section III the results of the different cases are compared and discussed in the view of the assessment of the different contributions to the electron current.

II. Numerical Model

The computational technique used is a standard electrostatic Particle-in-Cell/Monte Carlo Collision (PIC-MCC) model[6]. Operational input parameters used are those typical of an SPT-100 thruster.

The domain consists of the co-axial channel limited axially by the anode and the exit plane (forced to be at the cathode potential) and radially by the inner and outer walls. In order to lower the computational cost we have reduced the periodicity length to $\theta=\pi/2$ (clearly for cases A and C). Furthermore, a geometrical scaling[7] has been applied reducing the axial and radial dimension by f=10 and keeping constant all the most relevant non-dimensional

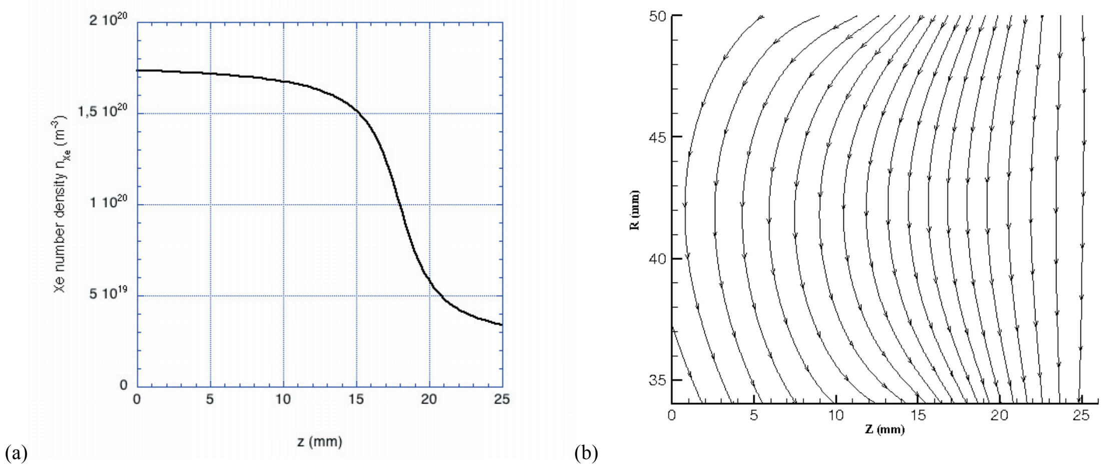

Figure 1. a) Xe atoms density distribution and b) magnetic field map used as fixed prescribed input data in the model.

Knudsen and Hall parameters. The volume of every cell is smaller than the Debye sphere and the time-step is chosen such that $\omega_p \Delta t$=0.3. Realistic values of the ion mass and vacuum permittivity have been kept.
A prescribed axial distribution (uniform in radial and azimuthal directions) of neutral Xe atoms density (Fig. 1.a):

$$n_{Xe}(z) = n_{Xe}(0) + 5x10^{18} \arctan\left[10\left(1 - \frac{z}{0.018}\right)\right] \tag{1}$$

($n_{Xe}(0)=1x10^{19}$ m^{-3} and z is expressed in meters) and magnetic field map (Fig. 1.b) (radial and axial components while B_θ=0) are imposed and fixed during the simulation.

The simulation starts from an empty domain. Electrons are introduced every time step from the exit plane with half-Maxwellian (T_{e0}=20 eV is used to simulate the electron acceleration occurring in the near-field plume region) velocity distribution. The amount of electrons injected inside the channel every PIC iteration is determined by subtracting the uneutralized positive ion current $I_{beam}=I_{Xe+,exit}+I_{Xe++,exit}$ exhausted to the current discharge ($I_{inj}=I_d-(I_{beam}-I_{e,exit})$). While the ignition has been rather simple for cases A and B, in the case C an extra injection of electrons has been necessary due to the complete loss of electrons (no SEE) inside the channel.

The Poisson equation in three-dimensional cylindrical geometry:

$$\left(\frac{\partial^2}{\partial r^2} + \frac{1}{r}\frac{\partial}{\partial r} + \frac{1}{r^2}\frac{\partial^2}{\partial \theta^2} + \frac{\partial^2}{\partial z^2}\right)\phi(r,\theta,z) = -\frac{\rho(r,\theta,z)}{\varepsilon_0} \tag{2.a}$$

is solved with Dirichelet fixed conditions on axial boarders at z=0 (anode) and at $z=L_z$ (cathode) such that all the acceleration is forced to occur inside the channel:

$$\phi(r,\theta)\big|_{z=0} = V_D; \quad \phi(r,\theta)\big|_{z=Lz} = 0, \tag{2.b}$$

while Neumann conditions are used on the insulating walls at $r=r_{in}$ and at $r=r_{out}$ (the possible surface conductivity of the dielectric is neglected):

$$\left.\frac{\partial\phi(\theta,z)}{\partial r}\right|_w \overset{def}{=} -E_{r,w}(\theta,z) = \pm\frac{\sigma_w(\theta,z)}{\varepsilon_0} \tag{2.c}$$

where + is for the outer wall and – is for the inner wall. Finally, periodic boundary conditions are set on azimuthal boundaries at θ=0 and at $\theta=\pi/2$.

$$\phi(r,z)\big|_{\theta=0} = \phi(r,z)\big|_{\theta=\pi/2} \tag{2.d}$$

Periodic conditions are used for particles crossing θ-boundaries. When an electron hits the dielectric channel wall (BN is simulated), in cases A and B we choose the number of electrons emitted based on its energy E_p. It is distinguished between three different types of secondary electrons: backscattered, re-diffused and true secondary electrons. A Monte Carlo probabilistic model[8] is used which allows a detailed dependence of the secondary electron emission coefficient γ on the primary electron energy E_p (see Fig. 2). Values of $\gamma(E_p=0)=0.44$ and $E_p(\gamma=1)=32$ eV have been used. While in case C all the electrons hitting the lateral walls are absorbed. Finally, when an ion strikes the wall it is neutralized and deleted from the list of particles tracked.

When electrons and ions leave the simulation domain from anode and cathode planes at z=0 and $z=L_z$, respectively, they are deleted from the list and a counter stores the number of particles in order to compute anode and cathode currents.

We apply the standard "null collision" Monte Carlo technique[9] to simulate electron-neutral (Xe) collisions, which include elastic scattering, excitation, and single ionization. Collisions producing Xe^{++} ions such as direct double ionization of Xe atoms and single ionization of Xe^+ ions have been also added.

III. Results

Table I summarizes the currents obtained for the different cases, and in particular, the electron current detected at the anode $I_{e,anode}$, and the total ion current detected at the exit plane $I_{i,exit-plane}$. Both values have been rescaled to the real value (in the geometrical scaling the current scales as f^2).

	Case A (3D)	Case B (2D)	Case C (3D-no SEE)
Electron current at anode $I_{e,anode}$ (A)	2.1	1.7	0.8
Ion current at cathode $I_{i,exit-plane}$ (A)	1.34	1.28	0.5

Table I – Summary of the currents detected for the different cases studied.

Comparing cases A and B, it is evident that the azimuthal fluctuation contributes to an increase of the cross-field electron current of 0.4 A, i.e. to the 20% of the total electron current. The comparison between cases A and C isolates the contribution of the secondary electron emission to the axial anomalous current, the so-called near-wall conductivity. With the secondary electron emission activated, the electron current goes from 0.8 A to 2.1 A, i.e. to an increment of 60% of the total current detected with the complete case A. This results shows that electron-wall interaction plays a relevant role, as already pointed out through different experimental measurements that have shown the influence of the different wall materials used to the current and efficiency detected.

In order to emphasize the complex structure of the electron transport inside the HET channel, the arrow-color map of electron current density $\boldsymbol{j}_e$ in the {r,z} plane (averaged over the azimuthal direction) has been reported in Fig. 2. The map shows the transition point located at z=2 cm between the forward flux (that neutralizing the ion flux emitted from the channel) and the backward flux moving towards the anode. A strong near-wall current is detected at the inner lateral surface in the acceleration region

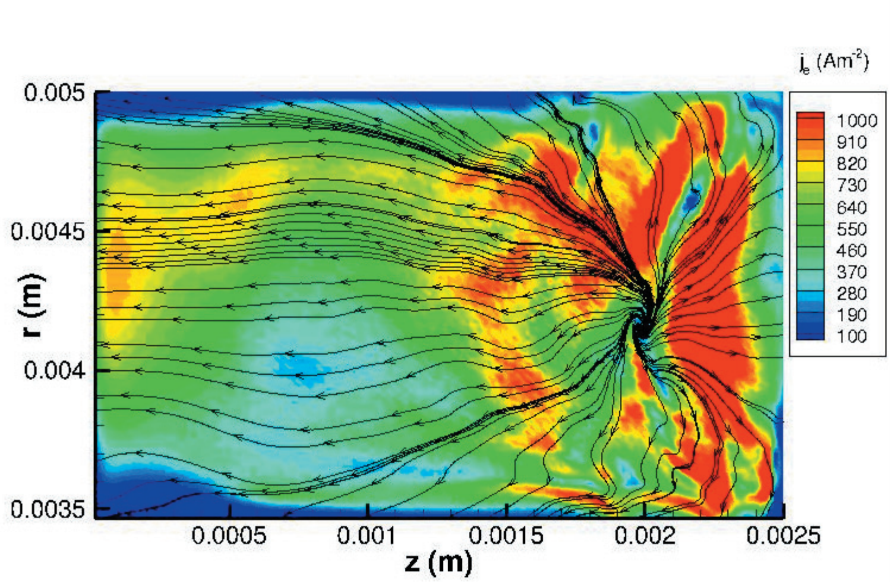

Figure 2. Arrow-color map of electron current density $\boldsymbol{j}_e$(A/m^2) in the {r,z} plane (averaged over the azimuthal direction).

Finally, the role of azimuthal fluctuation and secondary electron emission are evident in the maps of plasma potential in {r,z} (Fig. 3.a) and {r,θ} (Fig. 3.b) planes. It can immediately see the absence of space-charge-saturated regime sheath, often detected in reduced dimensionality (1D radial and 2D radial-axial or radial-azimuthal) models. It seembs that possibility to form three-dimensional sheath structure makes harder the occurance of non-classical sheath regiemes. Fig. 3.b shows the bulk azimuthal fluctuation characterized in the present scaled model by a wave nuber k_θ=770 m^{-1}.

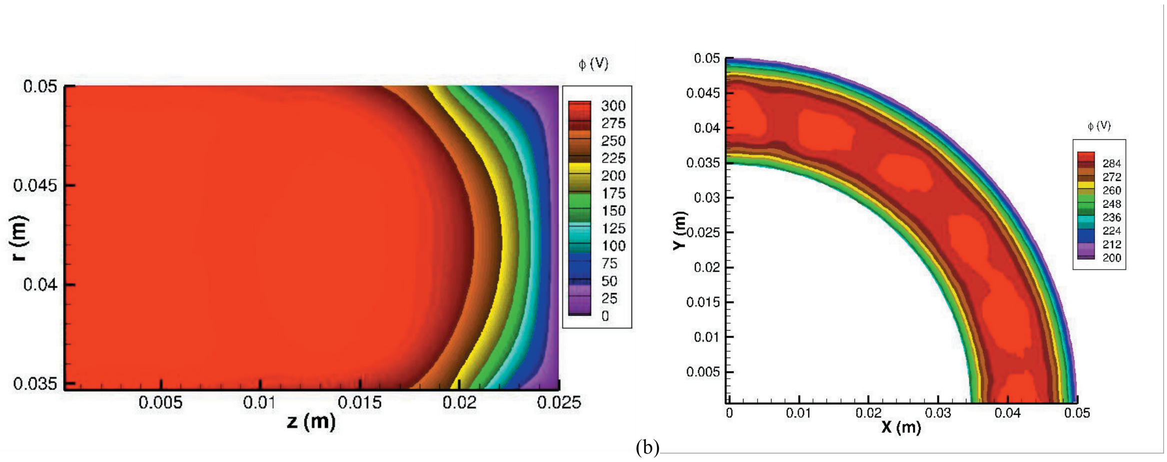

(a) (b)

Figure 3. a) {*r*,*z*} (at $\theta=\pi/4$) and b) {*r*, θ} (at *z*=2 cm) maps of electric potential ϕ(V).

IV. Conclusion

In this study the different contributions to the anomalous electron transport have been isolated by means of a numerical three-dimensional PIC-MCC model of the HET discharge. The model allows switching off the azimuthal direction and secondary electron emission from the lateral walls in turn. Results show the complex behavior of the electron current in the acceleration channel, pointing out the importance of electron-wall interaction, which contributes to 60% of the total electron current detected at the anode, while the azimuthal-induced current accounts for 20%.

Acknowledgments

This research has received funding by the project PON03PE000676 ApuliaSpace.

References

[1]Morozov, A. I., and Savel'ev, V. V., *Reviews of Plasma Physics* Vol. 21, ed. B. B. Kadomtsev and V. D. Shafranov, New York, 2000, pp. 203.

[2]Coche, P., and Garrigues, L., *Phys. Plasmas* Vol. 21, 023503, 2014.

[3]Héron, A., and Adam, J. C., *Phys. Plasmas* Vol. 20, 082313, 2013.

[4]Adam, J. C., Héron, A., and Laval, G., *Phys. Plasmas* Vol. 11(1), 295, 2004.

[5]Taccogna, F., Minelli, P., and Oudini, N., *IEPC-2013-148*.

[6]Tskhakaya, D., Matyash, K., Schneider, R., and Taccogna, F., *Contr. Plasma Phys.* Vol. **47(8-9)**, 563, 2007.

[7]Taccogna, F., Longo, S., Capitelli, M., and Schneider, R., *Phys. Plasmas*, Vol. 12, 053502, 2005.

[8]Furman, M. A., Pivi, M. T. F., *Phys. Rev. Special Topics–Accel. and Beams*, Vol. 5, 124404, 2002.

[9]Vahedi, V., Surendra, M., *Comp. Phys. Comm.,* Vol. 87, 179, 1995.